Detection of CO_2 using CNT-based sensors: Role of Fe catalyst on sensitivity and selectivity

CrossMark

Nacir Tit [a, *], Mohammed M. Al Ezzi [b], Hasan M. Abdullah [b], Maksudbek Yusupov [c],
Summayya Kouser [d], Hocine Bahlouli [b], Zain H. Yamani [b, e]

[a] Physics Department, UAE University, P.O. Box 15551, Al-Ain, United Arab Emirates
[b] Physics Department, King Fahd University of Petroleum and Minerals, P.O. Box 1690, Dhahran, 31261, Saudi Arabia
[c] Research Group PLASMANT, Department of Chemistry, University of Antwerp, Universiteitsplein 1, BE-2610, Wilrijk-Antwerp, Belgium
[d] Theoretical Sciences Unit, Jawaharlal Nehru Center for Advanced Scientific Research, Jakkur, Bangalore, India
[e] Center for Research Excellence in Nanotechnology, KFUPM, P.O. Box 5040, Dhahran 31261, Saudi Arabia

HIGHLIGHTS

- DFTB is used to study Adsorptions of CO_2 molecule on pG and CNT, with Fe catalyst.
- Armchair CNT-Fe has higher sensitivity to detect CO_2 than zigzag CNT-Fe and pG-Fe.
- Ac-CNT-Fe is highly sensitive and selective towards CO, CO_2 and H_2O gases.
- Keeping Fe ad-atoms dispersed and with low density enhances sensitivity.
- Our theoretical results corroborate the experimental findings of Ref. [8].

GRAPHICAL ABSTRACT
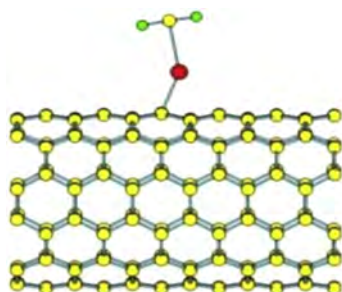
ARTICLE INFO

ABSTRACT

The adsorption of CO_2 on surfaces of graphene and carbon nanotubes (CNTs), decorated with Fe atoms, are investigated using the self-consistent-charge density-functional tight-binding (SCC-DFTB) method, neglecting the heat effects. Fe ad-atoms are more stable when they are dispersed on hollow sites. They introduce a large density of states at the Fermi level (N_F); where keeping such density low would help in gas sensing. Furthermore, the Fe ad-atom can weaken the $C{=}O$ double bonds of the chemisorbed CO_2 molecule, paving the way for oxygen atoms to drain more charges from Fe. Consequently, chemisorption of CO_2 molecules reduces both N_F and the conductance while it enhances the sensitivity with the increasing gas dose. Conducting armchair CNTs (ac-CNTs) have higher sensitivity than graphene and semiconducting zigzag CNTs (zz-CNTs). Comparative study of sensitivity of ac-CNT-Fe composite towards various gases (e.g., O_2, N_2, H_2, H_2O, CO and CO_2) has shown high sensitivity and selectivity towards CO, CO_2 and H_2O gases.

1. Introduction

Challenges resulting from global warming are forcing mankind to seek alternatives to traditional energy resources, such as the

* Corresponding author.
    E-mail address: ntit@uaeu.ac.ae (N. Tit).

renewable energy resources, as well as seek solutions to currently existing environmental problems [1]. Amongst plausible solutions is to search for suitable materials (of high efficiency and low cost) capable of capturing CO_2 gas molecule, which is one of the most important green-house gases, and to incorporate these materials into fabrication of devices such as sensors and filters for aim of environmental-safety and health-security applications. Generally, there are several basic criteria for good and efficient gas sensing systems: (i) high sensitivity and selectivity; (ii) fast response time and recovery time; (iii) minimal analyst intervention; (iv) low operating temperature, preferably at ambient temperatures; (v) stability in performance; and (vi) portability, as possible. In the last decade, research has focused on materials that control CO_2 emissions by capture and separation technologies, such as absorption, adsorption, membranes, and so forth [2]. These include adsorption technologies that use semiconducting metal oxides [3], zeolites [4], metal-organic frameworks (MOFs) [5], activated carbons [6], and other porous structured materials such as porous silicon [7]. In the recent years, several novel adsorbers of various atmospheric gases (including CO_2), such as carbon nanotubes (CNTs), graphene and graphene nano-ribbons (GNRs), have been experimentally and theoretically investigated as candidates for adsorption beds [8–15].

Carbon nanotubes have attracted enormous research interest since their discovery by Iijima in 1991 [16], due to their unique geometry, morphology, and other properties [17]. Their distinction from graphene, by virtue of their curvature properties, presents additional characteristics that are advantageous in the development of next generation high-speed electronic devices with properties exceeding those of silicon and conventional semiconductors. CNTs are categorized as materials possessing multi-functional characters with diversity of applications in various fields such as: (1) nano-electronics (e.g., synthesis of smallest transistors CNTFET) [18,19]; (2) photonics (e.g., utilization of CNTs in fabrications of LED [20] and dye-sensitized solar cells [21]); (3) biomedical field (e.g., CNTs in coatings [22]); (4) spintronics (e.g., the curvature can enhance spin-orbit coupling to yield spintronics) [23]; and (5) gas sensing (e.g., gas-sensors able to work at low temperatures) [24,25]. Graphene and CNTs are considered potential materials for gas-sensing that may even exceed the semiconducting metal oxides in sensitivity and selectivity towards certain gases and, thus, may gain a leading position in the field of gas-sensing [15,26–31].

To be specific, CNTs possess extremely high surface-to-volume ratio with high porosity (hollow structure), which are ideal for gas molecule adsorption and storage. In addition, the curvature permits relatively stronger binding with other ad-atoms or gas molecules. Keeping in mind that gas sensing principles relate to the adsorption and desorption of gas molecules on the sensing materials, it is quite understandable that by increasing the contact interfaces between the catalyst and the sensing materials, the sensitivity can be significantly enhanced. This has been demonstrated in the experimental work of Mishra and Ramaprabhu [32], who proved that chemisorption of CO_2 molecules on CNTs takes place only if the CNTs have been decorated with magnetite (Fe_3O_4) nanoparticles. These latter authors reported that such nanocomposites have the ability to be CO_2 absorbent with very high uptake capacity, much larger than that of activated carbon and much larger than zeolites, up to a temperature of about 100 °C. Further to this, a recent theoretical modelling used *ab-initio* calculations to study the absorption of H_2S on a ZnO 2D-honeycomb sheets and has noted the roles of metal catalysts in enhancing the chemisorption [33]. These authors compared four metal catalysts (Fe, Co, Pd and Au) deposited on a graphitic sheet of ZnO and found that iron yields the highest sensitivity and selectivity amongst the other metals because it has the least electro-negativity (i.e., the highest electro-positivity). Based on this, we have decided to use iron (Fe) as a catalyst deposited on CNT, and to assess the adsorption properties of CO_2 on the CNT-Fe composites.

The present work aims to study the adsorption properties of CO_2 molecules on both graphene and CNTs, in the presence of metal Fe catalysts. As a computational method, we employ the self-consistent-charge density-functional tight-binding (SCC-DFTB) technique, which uses DFT and has the ability to deal with large systems containing thousands of atoms, and perform accurate atomic relaxation in an efficient way [34,35]. The aim is also to relax Fe atom(s) on either graphene or armchair CNTs, then to relax CO_2 molecules on Fe ad-atoms. As output, we calculate the global-minimum total energy and obtain the fully relaxed structures as well as their corresponding band structures and density of states (DOS). From total energy calculations, one can estimate the binding energy of both Fe ad-atoms and CO_2 molecules. On the other hand, from DOS calculations, one can estimate the DOS at Fermi level from which conductance and gas detection sensitivity are evaluated. The selectivity is inspected by studying the sensitivity of ac-CNT-Fe composite to various gases (most of them are components of air, such as: N_2, O_2, H_2, H_2O, CO, and CO_2). A comparative study of selectivity includes a comparison with zigzag CNTs (i.e., zz-CNT-Fe compound) and graphene. This paper is organized as follows: Section 2 describes both the method and the models to be used in the computation. Section 3 gives a detailed discussion of the results. The last section summarizes our main findings.

2. Computational details and model systems

In the present work, three different systems have been modeled: (i) Graphene being modeled by a hexagonal supercell shown in Fig. 1b; the basis of which is a triangular lattice shown in Fig. 1a. In Fig. 1a, the vectors $\overrightarrow{a_1} = \frac{3}{2}a\hat{i} + \frac{\sqrt{3}}{2}\hat{j}$ and $\overrightarrow{a_2} = \frac{3}{2}a\hat{i} - \frac{\sqrt{3}}{2}\hat{j}$ are the lattice primitive vectors of pristine graphene structure, with a being the bond length $a = 1.42$ Å (i.e., note that the primitive cell contains 2 basis atoms of coordinates $\overrightarrow{r_1} = a\hat{i}$ and $\overrightarrow{r_2} = 2a\hat{i}$, respectively; and any other Bravais lattice site can be referred to by a vector $\overrightarrow{r} = n_1 \overrightarrow{a_1} + n_2 \overrightarrow{a_2}$, where n_1 nd n_2 are integers). We use a supercell composed of 6×6 primitive cells, containing 72 carbon atoms (i.e., $A = B = 6 \times 3a = 14.76$ Å, whereas the supercell c-axis is kept of size $C = 20$ Å, with a vacuum large enough to ensure the separation of adjacent periodic images of the sheet). In case of graphene, the Brillouin zone (BZ) was sampled using the Monkhorst-Pack (MP) technique [36], with a mesh of $26 \times 26 \times 1$ (i.e., 340 k-vectors were selected from within the irreducible wedge of the BZ and such number of k-vectors is tested to be sufficient to achieve the full convergences of both charge density and density of states "DOS"). (ii) Single-walled armchair CNT (ac-CNT) can be obtained by rolling the graphene sheet along the x-axis direction (i.e., along $\overrightarrow{r} = \overrightarrow{a_1} + \overrightarrow{a_2}$). In our present case, we have rolled the sheet along the vector $\overrightarrow{r} = 6\overrightarrow{a_1} + 6\overrightarrow{a_2}$ then repeated the ring structure for 6 periods along the tube axis (i.e., making an ac-CNT of radius R = 4.07 Å and length L = 14.76 Å; and the ac-CNT contains 144 carbon atoms). The length of the ac-CNT must be the size of the tetragonal supercell, used for computation, to ensure the validity of periodic boundary conditions along the tube. So, we use the tetragonal supercell, shown in Fig. 1c, of dimensionalities: $A = 14.76$ Å and $B = C = 20$ Å; this latter size is much larger than the radius of ac-CNT to ensure the complete isolation from adjacent periodic images of the tube. The sampling of the one-dimensional BZ is performed using MP technique with a mesh of $50 \times 1 \times 1$ (i.e., 26 k-vectors were selected from within the irreducible wedge to warrant full convergences of both charge density and DOS). (iii) Single-walled zigzag CNT (zz-CNT) can be obtained by rolling the graphene sheet along either $\overrightarrow{a_1}$ or $\overrightarrow{a_2}$ primitive graphene-lattice vectors. In our present case, we have rolled the graphene
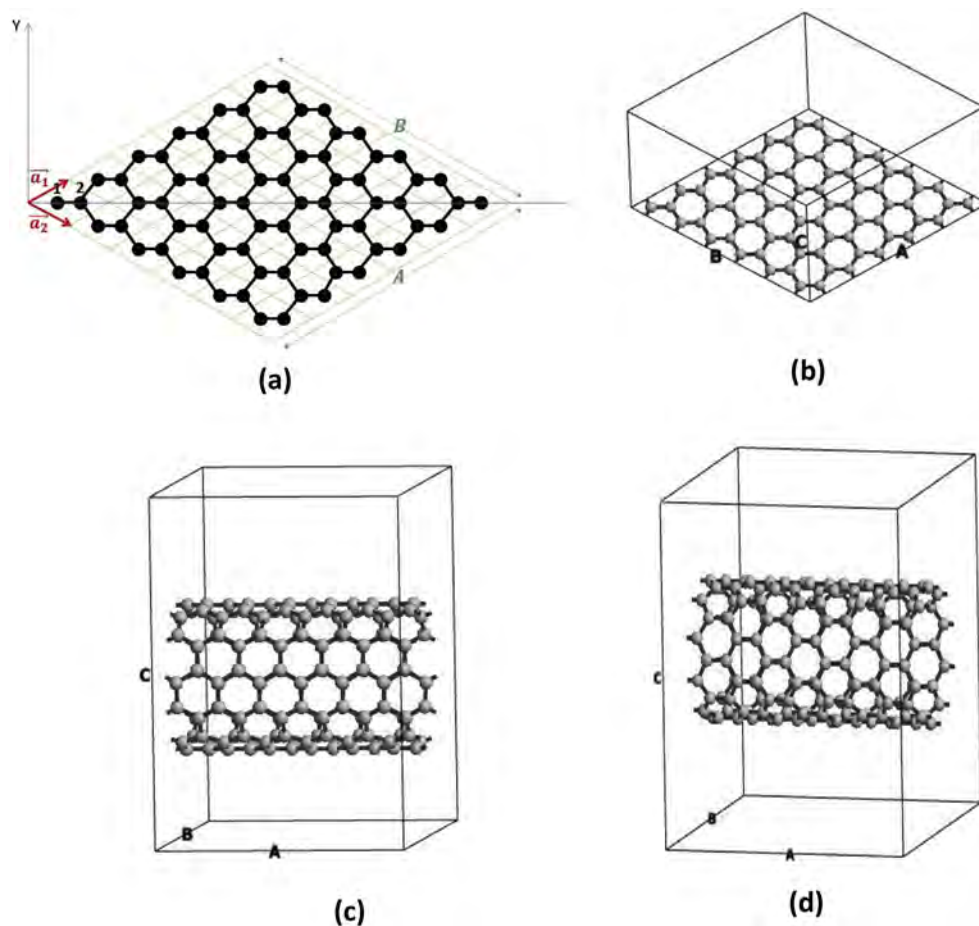
Fig. 1. (a) Pristine graphene sheet of size 6 × 6 primitive cells used in the calculations. The primitive lattice vectors ($\overrightarrow{a_1}$, $\overrightarrow{a_2}$) are shown. (b) Supercell of graphene; (c) Supercell of ac-CNT; and (d) Supercell of zz-CNT.

sheet along $\overrightarrow{r} = 10\,\overrightarrow{a_1}$ then repeated the ring structure for 4 periods along the tube axis (i.e., making zz-CNT of radius R = 3.92 Å and length L = 17.05 Å; containing 160 carbon atoms). Same procedures are taken regarding the supercell size and the BZ sampling as in the case of ac-CNT. The supercell of zz-CNT, which is used in one of our realizations in the present investigation, is shown in Fig. 1d.

In our computation, we investigate the adsorption properties of CO_2 molecule (and other molecules are studied for the aim of inspecting the selectivity) on the surfaces of the previously mentioned three systems in presence of Fe catalyst atom(s) in configuration of ad-atom(s). The relaxation processes are carried out mainly using the SCC-DFTB method [34,35], which is implemented in the DFTB + package. We use Slater-Koster (SK) parameter files [37] from the 'mio-0-1' [38,39] set to parameterize the inter-atomic interactions of carbon with other organic elements; whereas parameters of Fe's interactions with other elements are taken from the 'trans3d' [40]. van der Waals (vdW) interaction is accounted for by using the Lenard-Jones dispersion model used in DFTB+, with parameters taken from the universal force field (UFF). It is worth to emphasize that DFTB can deal with large systems containing hundreds to few thousands of atoms and efficiently carry out atomic relaxations. On one hand, approximating and parameterizing Fock-Matrix elements, an effective one-electron Kohn-Sham (KS) Hamiltonian is derived from density functional theory (DFT) calculations. On the other hand, DFTB is in close connection to tight-binding method. So, it can be seen as tight-

binding method, parameterized from DFT, and this overcomes the problem of parameters' transferability and makes the method more accurate. So, its basis set does not rely on plane-waves or Gaussian functions, but rather is a minimal basis set based on pseudo-atomic orbitals (Slater orbitals and spherical harmonics). Based on this basis set, DFTB gains its speed and ability to deal with large systems. So, in contrast to "full" DFT methods such as quantum Espresso, DFTB can easily handle calculations of large systems with reasonably large MP grid and perform atomic relaxations. Furthermore, DFTB was augmented by a self-consistency treatment based on atomic charges in the so-called self-consistent charge density-functional tight-binding (SCC-DFTB) method; charge density is expressed in terms of Milliken charges [41]. Because the wave functions in DFTB are well defined as KS-like orbitals, one can easily derive expressions for any property in the same way as within a "full" DFT scheme. This has indeed paved the way for DFTB to extend its domain of applications to even comprise biological systems [42]. Its strength stems from the transparent derivation, the inclusion of electron correlation on the DFT-GGA level and the updating parameterization process. This led to a robust method that predicts molecular geometries quite reliably. Among the limitations in DFTB is the availability of Slater-Koster files for all elements in the periodic table and this remains among the main challenges in the next years.

For the purpose of benchmarking the binding energy results, we explore another ab-initio code, which is quantum espresso (QE) package [43]. QE is based on DFT, plane-wave basis sets and

pseudopotentials (both norm-conserving and ultrasoft). In our particular study of adsorption of molecules on surfaces, as the charge density is expected to vary rapidly in space, we use a generalized gradient approximation (GGA) of Perdew Burke-Ernzerhof (PBE) parameterized form [44] and the interaction between ionic core and valence electrons is represented using ultra-soft pseudo-potentials [45]. Furthermore, we use Grimme scheme [46] to capture the long-range interactions namely van der Waals (vdW) like. We use plane-wave-basis set with energy cutoffs of 30 Ry and 180 Ry in representing orbital wave-functions and charge density, respectively. For the Brillouin-zone sampling, for instance in the case of sample of graphene, a uniform mesh of $5 \times 5 \times 1$ k-points is used, and the occupation numbers of electronic states is smoothened with a smearing width of order k_BT (i.e., about 0.04 eV) using Fermi-Dirac distribution function. Regarding the accuracy of the two methods, we carried out a small test of total energy calculations on a pristine graphene sample of size 5×5 primitive cells (i.e., containing 50 carbon atoms) and both DFTB and QE agree within a discrepancy of 10 meV when a relatively large MP mesh of about $12 \times 12 \times 1$ is used in QE code.

The atomic relaxed structures are determined via DFTB through the minimization of the total energy until Hellmann-Feynman force on each atom becomes smaller than 0.03 eV/Å in magnitude [47,48]. The atomic relaxation further comprises the relaxation of supercell lattice primitive vectors in order to release the stress and further minimizes the total energy. The calculation would, at the end, yield both the total energy and Fermi energy of the most stable geometry as well as its related total and partial densities of states.

The binding energy of the Fe ad-atom on the substrate is calculated using the following convention:

$$E_{bind} = E_{(Fe+substrate)} - E_{(substrate)} - E_{(Fe)} \qquad (1)$$

where $E_{(Fe+substrate)}$, $E_{(substrate)}$, and $E_{(Fe)}$ stand for the total energies of the relaxed Fe ad-atom on the substrate (here the substrate is either graphene or CNT), isolated substrate, and isolated Fe atom, respectively. We also define the adsorption energy of the CO_2 molecule on the adsorbent as follows:

$$E_{ad} = E_{(CO2+adsorbent)} - E_{(adsorbent)} - E_{(CO2)} \qquad (2)$$

where $E_{(CO2+adsorbent)}$, $E_{(adsorbent)}$, and $E_{(CO2)}$ stand for the total energies of system of CO_2 molecule and the adsorbent (the adsorbent can be either graphene-Fe composite or CNT-Fe compound), isolated adsorbent, and isolated CO_2 molecule.

In the case of adsorption of several molecules (for instance "N" molecules of CO_2), the average adsorption energy per molecule would be defined as

$$E_{ad}^{ave} = \frac{E_{(CO2+adsorbent)} - E_{(adsorbent)} - NE_{(CO2)}}{N} \qquad (3)$$

The *sensitivity* of a gas sensor is studied by looking at the variation of the electrical conductance versus gas dose (i.e., conductance versus number of molecules landed on the adsorbent). Appendix-1 shows the derivation of gas sensitivity and how it is related to density of states at Fermi level within the framework of free-electron gas.

Last but not the least, the *selectivity* is studied by keeping the gas dose constant but varying the gas type. All sensitivities are compared on a unified scale. In the present work, in case of studying the selectivity, we focus on ac-CNT decorated with just one Fe atom and sensitivity tests are carried out versus different gas molecules (namely, CO_2, CO, O_2, N_2, H_2, and H_2O). The results of structural relaxations, electronic structure calculations, and both

sensitivity and *selectivity* will be discussed in the next section.

3. Results and discussion

3.1. Atomic relaxations

The first assessment is of the stability of the Fe atom on both the pristine graphene and CNTs. As initial states, on graphene, an Fe atom was placed above the surface in three different positions within an expected Fe–C bond length and the system was allowed to relax. These three initial positions correspond to: (i) on-site, (ii) bridge-site and (iii) hollow-site positions. It was found that the hollow site position in both graphene as well as CNTs corresponds to the most stable configuration by having the lowest total energy. Specifically, we noticed that the binding energies corresponding to the mentioned three possible configurations of Fe ad-atom are ordered as follows: $E_{bind}^{Fe-onsite} = -1.279 eV > E_{bind}^{Fe-onbridge} = -1.314 eV > E_{bind}^{Fe-onhollow} = -1.412 eV$. The Fe on hollow-site is found to be the most stable configuration. Likely, the coordination of Fe and the number of bonds it makes with carbon atoms do matter in its stability on the graphene substrate. In addition to this, the adsorption energies of CO_2 molecule on Fe are also found to be in the same respective ranking. Hence, the results of just the two extreme cases (on-site and on-hollow-site) are selected and displayed in Tables 1 and 2. In the next step, a CO_2 molecule was placed just nominally above the Fe atom at a distance of about the C–Fe bond length from the Fe atom, after which, a second relaxation process was applied. Tracking the bond lengths and bond angles, the obtained converged configurations for both graphene and CNT clearly show evidence for chemisorption with the geometrical parameters shown in Table 1. The results for Fe positioned on on-site and hollow sites of graphene, as well as ac-CNT, are also shown for comparison. Focusing on the case of hollow sites, it is clear that ac-CNT-Fe compound exhibits stronger chemisorption with the CO_2 molecule than graphene-Fe composite does. Essentially, the surface-Fe and Fe–CO_2 distances are shorter in the case of CNT-Fe composite than those for graphene-Fe compound. Additionally, in the case of graphene, the CO_2 molecule possesses C–O bond length 1.17 Å, close to the value for the free molecule; and remains about linear with a bit distorted O–C–O angle of about 179°. On the other hand, the linearity and bond angle are much disturbed in the case of a CO_2 molecule on ac-CNT-Fe, where the C–O bond length (increased to 1.27 Å) became larger than the value for the free molecule; and the bond angle O–C–O decreased to about 154°. Thus, the double bonds O=C and C=O, in the CO_2 molecule after adsorption, are indeed weakened as π-bond broke down in paving the way for the molecule to have a stronger coupling/bonding to the Fe ad-atom.

From the point of view of energetics, Table 2A and B correspond to pristine graphene and ac-CNT, respectively. These Tables summarize the results for total energy, Fermi energy, binding energies of Fe on the surface, and CO_2 on Fe, density of states at Fermi level, gas sensing sensitivity, and average electronic charge of oxygen atom. Both Table 2A and B presents evidence that Fe on the hollow site is more stable than when it is on-site. Focusing on the hollow site cases, both the binding energy of Fe on the surface and the binding energy of CO_2 on the Fe ad-atom, in the case of ac-CNT, are much stronger than those in the case of graphene; these are consistent with shortening of both surface-Fe and Fe–CO_2 bond lengths, displayed in Table 1. Furthermore, the Fe atom introduces a huge DOS at Fermi level (N_F). Still, this N_F is more moderate in the case of ac-CNT (i.e., in ac-CNT, the atomic ratio is 1 Fe: 144 C atoms; whereas in graphene the atomic ratio is 1 Fe: 72 C atoms). These characteristics would make N_F in the case of ac-CNT to be more

Table 1

Comparison of geometrical parameters of four relaxed structures: (i) ac-CNT with 1 Fe (on-site) and 1 CO$_2$ molecule; (ii) graphene with 1 Fe (on-site) and 1 CO$_2$ molecule; (iii) ac-CNT with 1 Fe (on hollow site) and 1 CO$_2$ molecule; and (iv) graphene with 1 Fe (on hollow site) and 1 CO$_2$ molecule. Note that in the pictures: C, Fe and O atoms are shown in yellow, red and green colors, respectively.
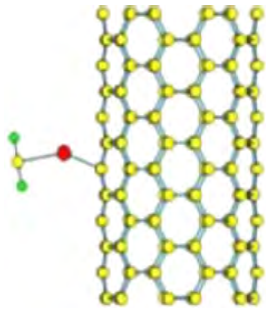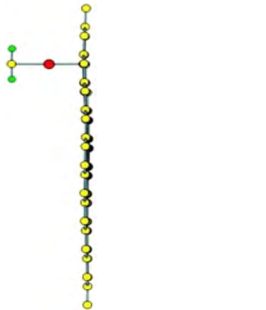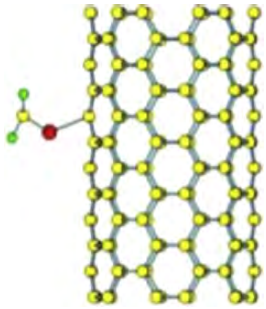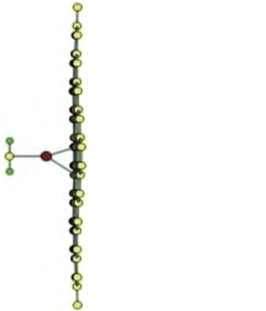
System	Fe on-site		Fe on hollow site	
	CNT–Fe–CO$_2$	G–Fe–CO$_2$	CNT–Fe–CO$_2$	G–Fe–CO$_2$
Relaxed structure				
D (Surf-Fe) Å	2.248	2.270	2.240	2.319
D (Fe–CO$_2$) Å	2.492	2.501	1.857	2.491
D (C=O) Å	1.172	1.172	1.272	1.172
Angle (Surf-Fe–C)	144.8°	178.6°	131.7°	154.5°
Angle (Fe–C–O)	89.2°	88.9°	76.7° & 129.5°	89.3°
Angle (O–C–O)	178.4°	177.7°	153.7°	178.5°

Table 2

Results of relaxations of 1 Fe atom on either on-site or on hollow-site as well as of 1CO$_2$ molecule on top of Fe ad-atom for: (A) Graphene and (B) ac-CNT.

A

System	On-site		On hollow site	
	G–Fe	G–Fe–CO$_2$	G–Fe	G–Fe–CO$_2$
E$_{TOT}$ (eV)	−3413.767	−3644.469	−3413.900	−3644.623
E$_F$ (eV)	−4.254	−4.219	−4.224	−4.195
E$_{bind}$ (eV)	−1.279	−2.075	−1.412	−2.096
N$_F$ (1/eV per Hexagon)	0.4941	0.4738	0.3248	0.2840
Sensitivity (%)	N/A	4.11%	N/A	12.56%
Charge of O atom (e units)	N/A	6.328	N/A	6.330

B

System	On-site		On hollow site	
	CNT–Fe	CNT–Fe–CO$_2$	CNT–Fe	CNT–Fe–CO$_2$
E$_{TOT}$ (eV)	−6777.891	−7008.719	−6778.013	−7009.358
E$_F$ (eV)	−4.367	−4.313	−4.339	−4.503
E$_{bind}$ (eV)	−1.559	−2.200	−1.680	−2.718
N$_F$ (1/eV per Hexagon)	0.2480	0.1764	0.2057	0.1340
Sensitivity (%)	N/A	28.3%	N/A	34.85%
Charge of O atom (e units)	N/A	6.3395	N/A	6.3991

sensitive to the landing of CO$_2$ on Fe than for graphene. In other words, the variation of DOS at Fermi level, before and after the landing of CO$_2$ on an Fe ad-atom, is considerably larger in the case of ac-CNT than on the case of graphene. Fig. 2 corroborates the observation of DOS at Fermi level. It shows that the shape of the CO$_2$ molecule deviates from its original linearity when it gets adsorbed on ac-CNT-Fe compound more than when it get adsorbed on graphene-Fe compound. One final remark is that the average charge of the oxygen atom in the case of ac-CNT is also larger than that in the case of graphene, because oxygen is more electronegative than carbon and as the O=C and C=O double bonds weaken (i.e., π-bond breaks down) on ac-CNT, oxygen atoms will get the opportunity to drain more charge and reduce the DOS at Fermi level, consequently causing more surface resistance and higher sensitivity. A rough estimate of sensitivity shows that in ac-CNT-Fe composite, it is about 35% compared to 12.5% in case of graphene-Fe compound of similar concentrations. This stimulated us to focus more on CNTs for the remainder of the investigation.

One further use of graphene in this investigation was to assess the effect of metal ad-atom clustering on the sensitivity. To this aim, in our model we have first relaxed the group of 5 Fe atoms on a graphene super-cell of 6 × 6 primitive cells in three different configurations: (i) linear chain of Fe-atoms; (ii) planar cluster of Fe-atoms and (iii) scattered Fe-atoms. Then, we deposited and relaxed CO$_2$ molecules on the Fe ad-atoms. We found that the average binding energies, surface-Fe distance, and Fe–CO$_2$ distance have minimal values in the case of scattered configuration of Fe ad-atoms. The sensitivity in the latter configuration is much higher because the Fermi level becomes populated with a lower density of localized states originating from the Fe metal atoms. Based on these findings, we decided to deal with scattered Fe atoms on the CNT surface and study the variation of sensitivity versus gas dose for the ac-CNT-Fe composite.

To study the sensitivity as a function of CO$_2$ gas dose, the first step was to relax 5 Fe ad-atoms that were initially scattered on the surface of ac-CNT. Then, we relaxed 5 CO$_2$ molecules that were originally positioned above the Fe ad-atoms, in a consecutive way, one after the other (making a total of five different samples to be relaxed). Fig. 3a shows the relaxed configurations of (ac-CNT + 5 Fe atoms) and Fig. 3b and c shows two among the mentioned 5 samples, which include CO$_2$ molecules. These latter two samples
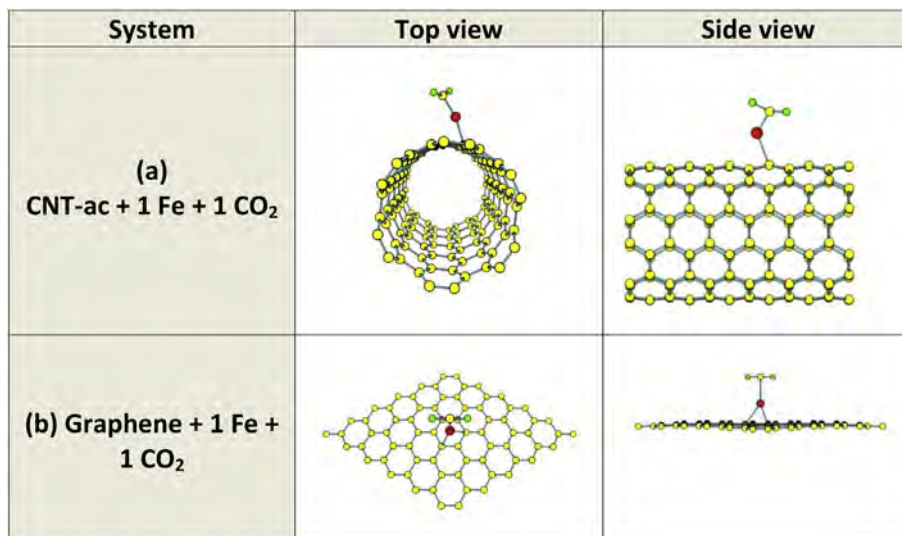
System	Top view	Side view
(a) CNT-ac + 1 Fe + 1 CO$_2$		
(b) Graphene + 1 Fe + 1 CO$_2$		

Fig. 2. Comparison between relaxed atomic structures of two systems showing the chemisorption of CO$_2$ on: (a) ac-CNT with 1 Fe ad-atom, and (b) Pristine graphene with 1 Fe ad-atom. Note that in both latter cases Fe ad-atoms are placed on hollow sites. Note that C, Fe and O atoms are shown in yellow, red and green colors, respectively. (For interpretation of the references to colour in this figure legend, the reader is referred to the web version of this article.)
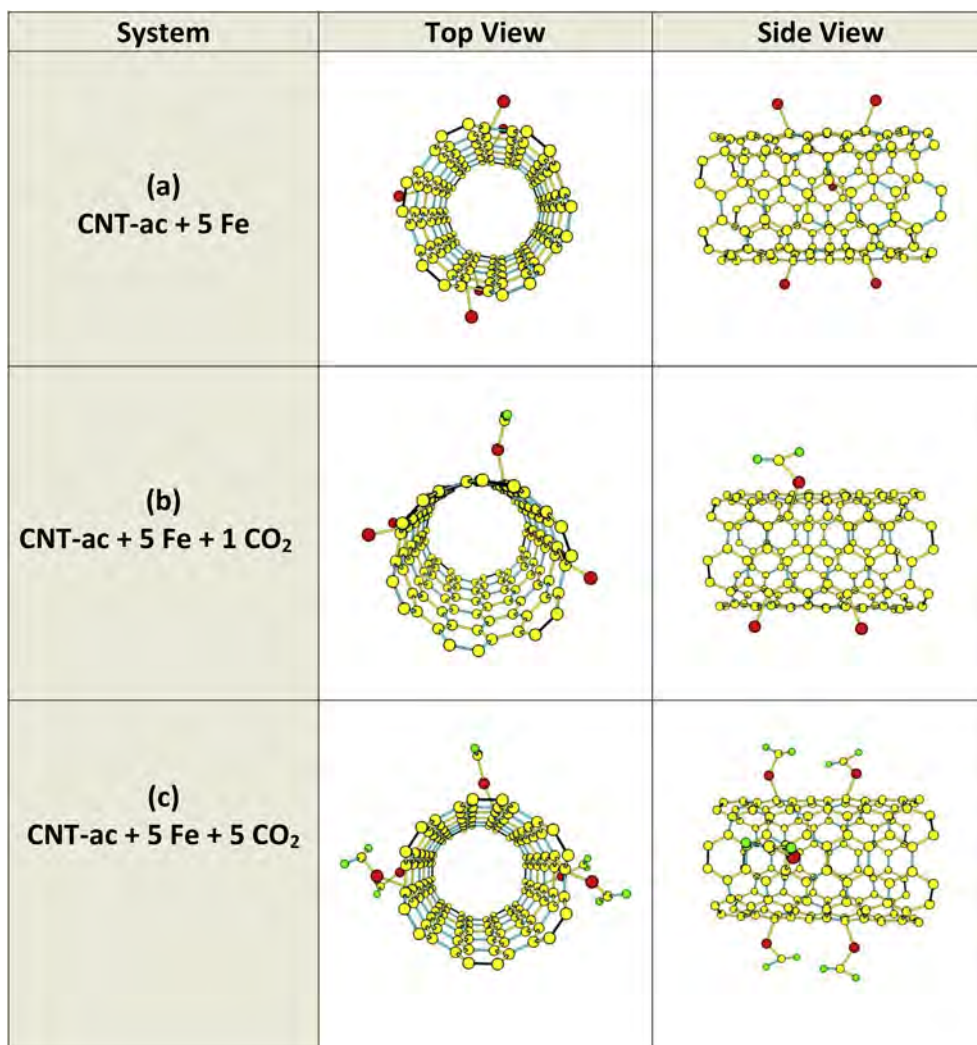
System	Top View	Side View
(a) CNT-ac + 5 Fe		
(b) CNT-ac + 5 Fe + 1 CO$_2$		
(c) CNT-ac + 5 Fe + 5 CO$_2$		

Fig. 3. (a) Relaxed atomic structures of ac-CNT with 5 Fe ad-atoms dispersed on its surface before the arrival of CO$_2$ gas molecules, (b) After chemisorption of 1 CO$_2$ molecule, and (c) After chemisorption of 5 CO$_2$ molecules.

are: (2b) ac-CNT + 5 Fe + 1 CO_2 and (2c) ac-CNT + 5 Fe + 5 CO_2. Basically, the configuration and geometry of CO_2 are independent of gas dose and remain similar to those in the case of (ac-CNT + 1 Fe + 1 CO_2), shown in Fig. 2. However, the increase in the number of CO_2 molecules would allow oxygen to drain more electrons from the Fermi level after the weakening of O=C and C=O bonds (breaking of π-bonds) of the adsorbed CO_2 molecule. The reduction of the DOS at Fermi level with the increasing number of CO_2 molecules would yield more surface resistance and, thus, greater sensitivity due to the enhanced variations in the DOS at Fermi level.

3.2. Study of sensitivity

Fig. 4a displays the partial densities of states (PDOS) and the total densities of states (TDOS) of the system composed of ac-CNT (containing 144 carbon atoms), 5 Fe atoms and 1 CO_2 molecule. This latter molecule has been chemisorbed on one of the five iron atoms. PDOS contributions of C, Fe, O atoms are shown in Fig. 4a in black, blue, and green curves, respectively. The five metal Fe ad-atoms, in fact, introduce a huge DOS at the Fermi level, as well as spread DOS along the conduction band (i.e., energy range [−1, +8] eV). The DOS of Fe atoms being spread over the conduction band (CB) reveals the formation of bonds with carbon atoms of CNT. Fig. 4b shows the TDOS of 6 systems containing zero to five CO_2 molecules, after they have been relaxed on the available five Fe ad-atoms. The energy range [−1.5, 1.5] eV is concentrated around the Fermi level, which is taken to be the common energy reference for all of the 6 composites. Fig. 4b shows clearly the decrease of DOS at Fermi level (N_F) associated with increasing number of CO_2 molecules getting attached to Fe ad-atoms on the CNT's surface. This reduction of DOS at Fermi level is caused by the effect of chemisorption of CO_2 molecules on Fe atoms, as described in the previous sub-section. The double bonds of O=C and C=O weaken, as π-bonds break down, paving the way to oxygen atoms to drain more charge from the Fe atoms. Furthermore, it was emphasized that the change of DOS at Fermi level due to the landing of CO_2 molecules is also sensitive to the clustering of Fe atoms and their ratio to the total number of carbon atoms in CNT.

Fig. 5 summarizes the results of variations of DOS at Fermi level, sensitivity, and average charge of oxygen atom versus the gas dose
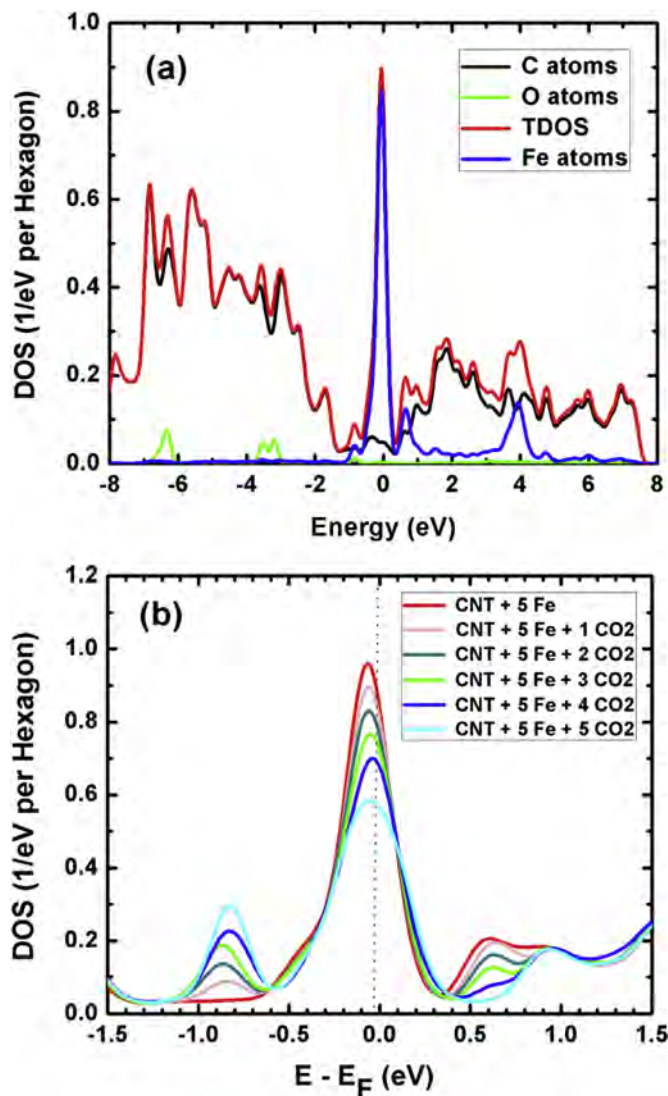

Fig. 4. (a) TDOS and PDOS of a relaxed system of ac-CNT with 5 Fe ad-atoms and 1 CO_2 molecule on its surface are shown. (b) TDOS of 6 systems: each consisting of ac-CNT and 5 Fe ad-atoms on its surface as well as CO_2 molecules, the number of which is varied between 0 and 5. Fermi level is taken as an energy reference in both panels.
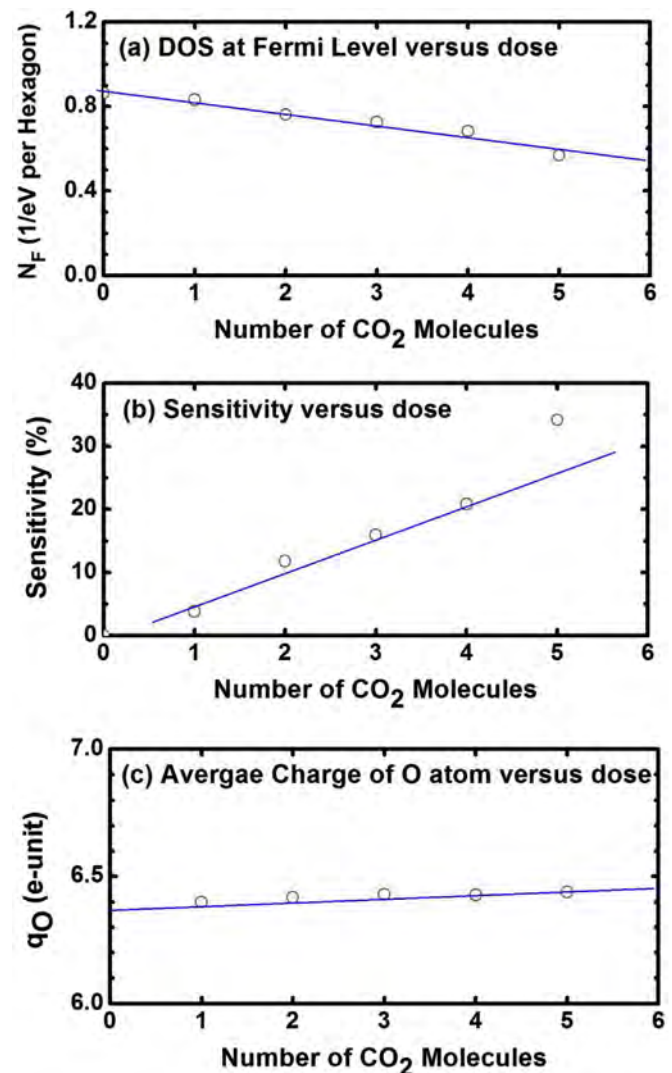
Fig. 5. (a) DOS at Fermi level, (b) Sensitivity, and (c) Average charge of O atom versus the number of CO_2 molecules chemisorbed on a surface of the ac-CNT with 5 Fe ad-atoms.

(with the number of CO_2 molecules varying from 0 to 5). Fig. 5a shows a linear decrease of N_F against the number of CO_2 molecules. Consequently, the conductance is expected to decrease as the number of CO_2 molecules increases. In addition to this, the sensitivity increases with the increasing CO_2 gas dose, as shown in Fig. 5b. Fig. 5c corroborates the plot of sensitivity versus gas dose by showing the increase in the average charge of oxygen atoms versus dose. Oxygen atoms are more electronegative than carbon atoms and should drain more charge from the system after the occurrence of chemisorption of various CO_2 molecules on Fe atoms.

In order to show the evidence of occurrence of both bonding and charge transfer from the adsorbent to the CO_2 molecule. We took the case of graphene-Fe compound as adsorbent. Fig. 6 displays the charge-density plots of the valence-band-edge and conduction-band-edge eigen-states' magnitudes (i.e., so named in chemistry highest-occupied molecular orbital "HOMO" and lowest-occupied molecular orbital "LUMO" states). Both top view and side view are shown. The C, Fe and O atoms are shown in grey, red and green colors, respectively. The HOMO and LUMO eigen-states are shown in blue color. The side view of HOMO state is shown to be delocalized over all sites including all C, Fe and O atoms. This reveals the occurrence of covalent bonding. Whereas, the side view of LUMO state is shown to be distributed over all sites but not the CO_2 molecule. This reveals that the CB-edge has permissible states to accommodate more charge transfers as behaving like the role of a cationic electro-positive element. In brief, the occurrence of bonding of CO_2 molecule with Fe is obviously shown through the HOMO state. Such charge transfer occurring from surface to molecule has also been reported in the Bader analysis reported by Bendavid and Carter [12], where transfer of charge occurs from CuO_2 surface to the adsorbed CO_2 molecule, and more efficiently on V_{Cu} site.

3.3. Effect of energy gap on sensitivity

We have considered two types of CNTs having two different electrical characteristics; namely: (i) ac-CNT containing 144 carbon atoms, representing an example of a conducting CNT, and

containing a single Fe ad-atom on a hollow site; and (ii) zz-CNT containing 160 carbon atoms of geometry 10×4 avoiding multiples of 3 in circumference, in order to make it a suitable representative of a semiconducting CNT. The calculated band-gap energy for this latter zz-CNT is found to be 1.143 eV, in the absence of Fe ad-atom. Then, on the top of each Fe ad-atom of CNT, a CO_2 molecule is deposited and relaxed. We quote that in displaying the band structures, the energy reference is taken to be the vacuum level so that one can follow the changes introduced by adding 1 Fe atom on a hollow site of the CNT, and also subsequent changes introduced by adding 1 CO_2 molecule on Fe ad-atom. On the other hand, in DOS plots, the Fermi level is taken as the common energy reference. The order in each panel is performed to correspond to: (1) Pure CNT, (2) CNT with 1 Fe ad-atom after relaxation, and (3) CNT with 1 Fe ad-atom and above it a chemisorbed CO_2 molecule, after relaxation process.

For the ac-CNT, Fig. 7a displays the bands along the ⌈X-high symmetry line for three relaxed structures: (a1) pure CNT, (a2) CNT + 1Fe, and (a3) CNT + 1Fe + 1CO_2. Panel (a1) shows two bands crossing at Fermi level to yield a conducting CNT. Panel (a2) shows the shift of Fermi level towards the states introduced by the Fe ad-atom. Many bands above Fermi level originating from the Fe atom apparently lack dispersion (as they correspond to localized states on d orbitals of Fe). Panel (a3) shows the effect of chemisorption of CO_2 on the Fe atom in making some localized d-states coupled to the CO_2 molecule. The corresponding DOS to these three structures is shown in panels b1 to b3, respectively. Panel b1 shows a flat DOS at Fermi level (in the energy range $[-1, 1]$) revealing the metallic character of this ac-CNT. Panel (b2) shows that the Fe ad-atom introduces a large DOS at Fermi level, of more than 0.20 states/eV per hexagon for each single Fe ad-atom. Panel (b3) shows that the chemisorption of CO_2 molecule reduces the DOS at Fermi level to about 0.13 states/eV per hexagon. Thus, the sensitivity produced is enormous of about 35%.

In the case of zz-CNT, Fig. 7c displays the bands for three relaxed structures as follows: (c1) pure CNT, (c2) CNT + 1Fe, and (c3) CNT + 1Fe + 1CO_2. Panel (c1) shows an energy bandgap of about 1.143 eV with Fermi level lying in the middle of the gap. Panel (c2)
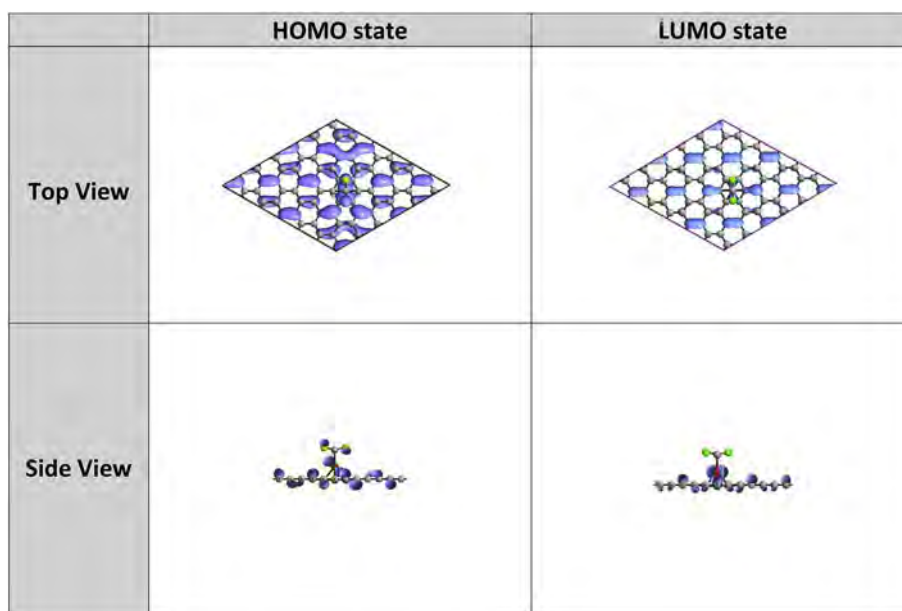

	HOMO state	LUMO state
Top View		
Side View		

Fig. 6. Charge density plots presenting the magnitudes of the HOMO and LUMO states in Graphene-Fe−CO_2 systems. Colors used for: C (grey), Fe (red), and O (green); while the eigen-states are in blue color. (For interpretation of the references to colour in this figure legend, the reader is referred to the web version of this article.)
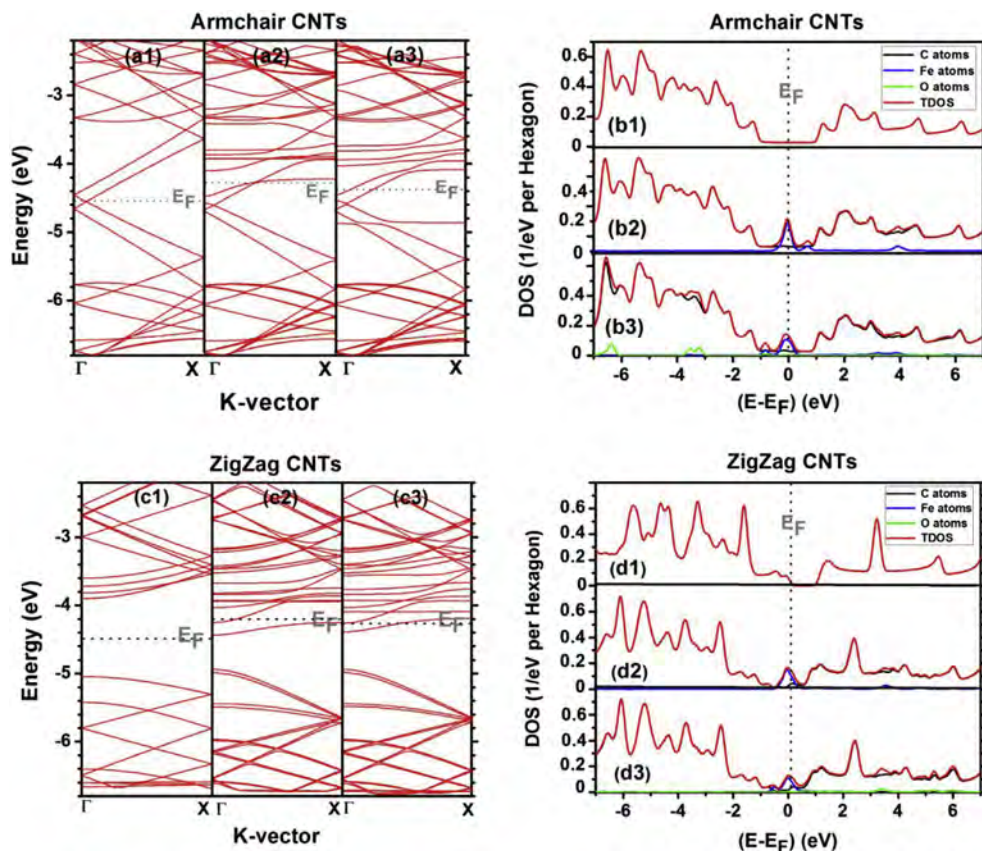
Fig. 7. Comparison of band structures and DOS of ac-CNT (containing 144 carbon atoms) and zz-CNT (containing 160 carbon atoms). The numbers associated to letters stand for: (1) pure CNT, (2) CNT with 1 Fe ad-atom, and (3) CNT-Fe compound after chemisorption of 1 CO_2 molecule. In the bands, vacuum level is taken as an energy reference. Whereas, for DOS, either Fermi level (E_F) or valence-band edge (E_V) is taken as an energy reference. TDOS is normalized to 8 electrons per hexagon in case of pure CNT.

shows that the Fe ad-atom introduces both delocalized states due the bonding with CNT, and localized d-states likely due to dangling bonds. Nevertheless, the Fermi level is shifted to lie on Fe states below the conduction-band edge of zz-CNT. Panel (c3) shows the effect of chemisorption of CO_2 molecule on the Fe ad-atom. The Fermi level continues to lie on Fe states below the conduction-band edge of zz-CNT (i.e., mobility edge). Hence, one expects a poor conductivity and consequently less sensitivity. As an over-estimation, the sensitivity of zz-CNT would not exceed 22%. As a matter of fact, this latter system does not reach the necessary values of conductivity to validate the Drude formula. Fig. 7d shows the DOS corresponding to the three structures of Fig. 7c. The Fe ad-atom introduces a large DOS at Fermi level of about 0.16 states/eV per hexagon. The chemisorbed CO_2 molecule on the Fe ad-atom reduces this DOS to become about 0.13 states/eV per hexagon. However, this DOS at Fermi level is due to states, which are still very localized on the Fe atom and should not contribute to conductivity

as $E_F < E_C$ (zz-CNT); i.e., below mobility edge. This, in turn, will make the sensitivity of zz-CNT much lower than that of ac-CNT. Table 3 summarizes a quantitative comparison of the obtained results between ac-CNT and zz-CNT.

3.4. Study of selectivity

To study selectivity, we have considered the ac-CNT containing 144 carbon atoms, with one Fe ad-atom relaxed on a hollow site. Following this, we performed relaxations above this Fe ad-atom of various gas molecules (namely: O_2, N_2, H_2, H_2O, CO and CO_2), in addition to the adsorption of CO_2 molecule on graphene-Fe and on zz-CNT-Fe. Fig. 8a displays a bar chart of the binding energy of CO_2 and other gases while Fig. 8b displays the sensitivity of same gases on CNT-Fe compound. Table 4 summarizes some geometrical parameters of the converged structures. All molecules endure chemisorption processes except N_2 which exhibits physisorption. It

Table 3
Results of relaxation of 1 Fe atom on hollow sites of both zz-CNT and ac-CNT (for sake of comparison), followed by the relaxation of 1 CO_2 on the Fe ad-atom.

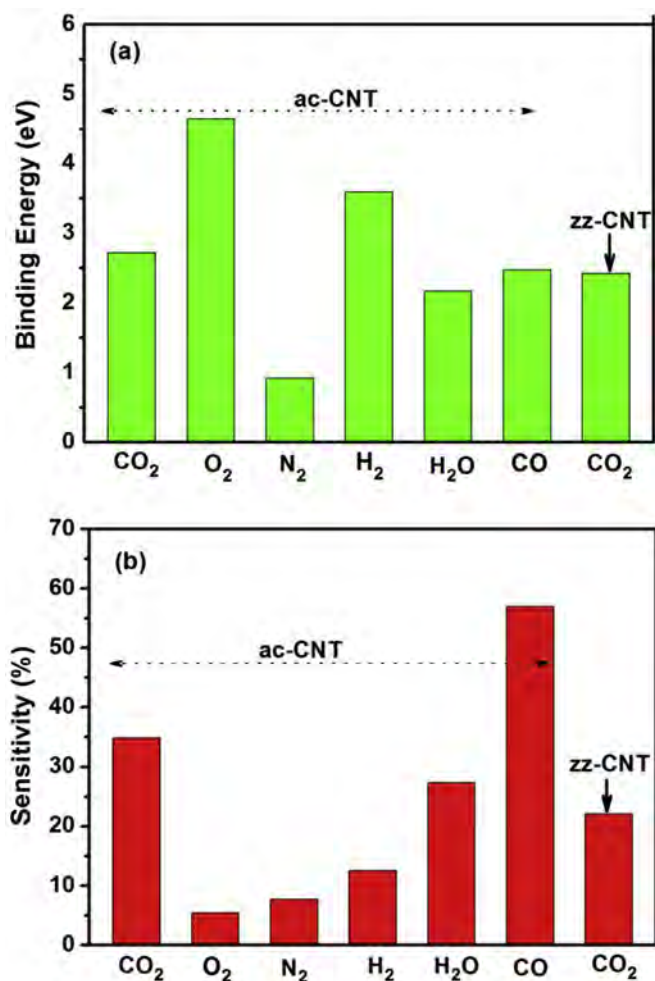| System	Zigzag		Armchair	
	CNT–Fe	CNT–Fe–CO_2	CNT–Fe	CNT–Fe–CO_2
E_{TOT} (eV)	−7526.305	−7757.358	−6778.289	−7009.630
E_F (eV)	−4.206	−4.397	−4.344	−4.506
E_{bind} (eV)	−1.511	−2.426	−1.701	−2.714
N_F (1/eV per Hexagon)	0.165	0.130	0.206	0.135
Sensitivity (%)	N/A	22.42%	N/A	34.64%
Charge of O atom (e units)	N/A	6.387	N/A	6.399

Fig. 8. Bar chart of the binding energy in green color (a) of a single gas molecule and the gas sensitivity in red color (b) versus different gases is shown. The adsorbent is ac-CNT with 1 Fe ad-atom. (For interpretation of the references to colour in this figure legend, the reader is referred to the web version of this article.)

plausible. Moreover, one should emphasize that the sensitivity in the case of zz-CNT towards detecting CO_2 (values are displayed in Table 4) is overestimated because the studied zz-CNT is a semi-conductor and Drude model should not be valid. Yet the sensitivity of zz-CNT remains much lower than the one of ac-CNT. In case of O_2 molecule, Fe is able to break one of the O=O double bond (specifically, the π-bond breaks down) and able to make a sigma bond with each of the two oxygen atoms without dissociating the O_2 molecule. The last molecule to discuss its chemisorption on ac-CNT is H_2O. The O atom makes a bond with Fe ad-atom while it maintains the other two bonds with its two H atoms. Nonetheless, it seems to have comparable binding energy and sensitivity to those of CO_2. In summary, the ac-CNT decorated with Fe metal catalyst is highly sensitive and selective towards the detection of CO_2, CO and H_2O gases.

4. Conclusions

The self-consistent-charge density-functional tight-binding (SCC-DFTB) method was employed to study the adsorption properties of CO_2 molecules on both pristine graphene and pure conducting ac-CNT, after being decorated with Fe metal-catalyst atoms. It was found that the catalyst plays a crucial role in inducing and enhancing the interaction to a level of achieving chemisorption state. The results of chemisorption of CO_2 molecule on G-Fe and ac-CNT-Fe compounds can be summarized as follows:

(1) It is recommended to deposit Fe atoms in a scattered manner on the surface of graphene or CNT, since any clustering of Fe atoms yields less binding to the surface and less coupling with CO_2 molecules. Thus, the clustering is found to yield lower sensitivity. The Fe atoms should be scattered and their ratio should be restricted with respect to the total number of existing carbon atoms. The optimum number should not exceed the order of a doping density in semiconductors (i.e., much less than 1% of total number of carbon atoms). Below that limit, Fe will enhance the DOS at Fermi level and lead to considerable reduction of N_F by the chemisorption of CO_2 molecules. The reduction of N_F will enhance both the surface electrical resistance and sensitivity versus gas dose.
(2) The atomic relaxations demonstrate that the deposition of Fe on hollow site yields the most stable configuration. Additionally, the ac-CNT were found to have sensitivity much higher than those of graphene and zz-CNT. Thus, our study of sensitivity and selectivity was focused only on ac-CNT.
(3) In the study of sensitivity, CO_2 molecules were deposited on ac-CNT-Fe compound one by one (N = 0–5 molecules). N_F was found to decrease, resulting in enhancement of resistance and sensitivity. The C=O double bonds were found to partially break down and become weaker and longer than those in free CO_2 molecule. The O–C–O angle was found to decrease to 154° (this angle is likely dependent on curvature). Meanwhile, the average charge of oxygen increases

seems that the triple bond N≡N is so strong and stable that the molecule N_2 does not prefer interacting even with a metal catalyst. At the other extreme, H_2 molecule exhibits chemisorption with dissociation. The Fe atom is able to split H_2 and make two separate Fe–H single bonds. In case of CO chemisorption, the oxygen atom is found to be the one to bond to Fe ad-atom instead of C atom. This is because O atom is more electronegative than C atom. On the other hand, in the chemisorption of CO_2 molecule, this latter breaks its linear shape as C=O bonds get weaker (due break down of π-bonds) in paving the way for the molecule to couple with Fe ad-atom. The fact that this chemisorption occurs without dissociation of molecule would suggest that the recovery process is

Table 4
Results of selectivity analysis of CO_2, O_2, N_2, H_2, H_2O and CO gases are shown. The results include: the Fe-molecule distance, angular distortion of molecule, binding energy of molecule and type of adsorption.

Molecule	D (Fe-molecule) (Å)	Angle (degrees)	Type of adsorption	E_{bind} of molecule (eV)	Comment about molecule
CO_2	1.857	O–C–O: 153.7°	Chemisorption	−2.718	No split: Fe–C bond is the shortest
O_2	1.938	O–Fe–O: 54.2°	Chemisorption	−4.639	No split: O–Fe–O is isosceles triangle
N_2	2.582	N–Fe–N: 25.2°	Physisorption	−0.923	No Split: both N atoms are equidistant to Fe
H_2	1.531	H–Fe–H: 95.2°	Chemisorption	−3.586	Split
H_2O	1.942	H–O–H: 106.3°	Chemisorption	−2.169	No split: D (Fe–H) = 1.699 Å is the shortest
CO	1.686	O–C–Fe:89.6°	Chemisorption	−2.472	No split: Fe–C bond is the shortest

against gas dose, because oxygen has higher electronegativity than carbon and would drain more charge from Fe atom with increasing gas dose.

(4) On the issue of selectivity, ac-CNT-Fe compound was found to be highly sensitive and selective towards three gases (CO, CO_2 and H_2O) to a greater degree than any other gas studied (such as O_2, N_2, H_2). The cost of production of ac-CNT-Fe systems being relatively low, would make them promising candidates for mass production of ac-CNT-Fe based sensors, filters, and storage devices.

Acknowledgements

Appendix. Metallic conductivity and gas sensitivity

In a free-electron gas, such as in metals, Ohm's law relates the current density to the electric field ($\mathbf{j} = \sigma\mathbf{E}$, where σ is the electric conductivity). Within the picture of the classical Drude's model [49], the only possible interaction of a free electron with its environment is through instantaneous collisions. The average time between subsequent collisions is τ, and conductivity is given by the formula:

$$\sigma = \frac{ne^2\tau}{m} = ne\mu \qquad \text{(A-1)}$$

where n is the number density of free electrons, e and m are charge and mass of free electron, and μ is the electron mobility. This formula is derived under assumptions of application of static electric field and uniform temperature.

It should be further emphasized that the above conductivity depends only on the properties of the electrons at the Fermi surface, not on the total number of electron in the metal. The high conductivity of metals is to be ascribed to the high current, $\mathbf{j_F} = ne\mathbf{v_F}$, carried by the few electrons at the top of the Fermi distribution, rather than to the total density of free electrons (i.e, $\mathbf{v_F}$ is Fermi velocity, and electrons of lower energy than Fermi energy are slowly drifting). Thus, the electrical conductivity gains its main contribution from states near Fermi surface and may be written as [50]:

$$\sigma = \frac{1}{3}j_F^2\tau g(E_F) \qquad \text{(A-2)}$$

where $g(E_F)$ is the density of states at Fermi level and E_F is Fermi energy.

From another perspective, using free-electron model at $0\ °K$ temperature, the density of states at Fermi level is given [49] by:

$$g(E_F) = \frac{3n}{2E_F} \qquad \text{(A-3)}$$

Furthermore, it should be emphasized that in Ohm's law, the resistance R is connected to the resistivity ρ by:

$$R = \rho\frac{L}{A} \qquad \text{(A-4)}$$

where L and A are the length and cross-sectional area of the sample. The counter-part of resistance is the conductance (G = 1/R) and the counter-part of resistivity is conductivity ($\sigma = 1/\rho$); so the conductance may be written as:

$$G = \sigma\frac{A}{L} \qquad \text{(A-5)}$$

In gas-sensing, the concept of gas sensitivity "S" is based on the variation of resistance between two states (before and after exposure to gas). It is customary to define the sensitivity as follows [51–53]:

$$S = \frac{|I_g - I_a|}{I_a} \times 100\% = \frac{|R_g - R_a|}{R_g} \times 100\% = \frac{|G_g - G_a|}{G_a} \times 100\% \qquad \text{(A-6)}$$

where the pairs of I_g, I_a and R_g, R_a and G_g, G_a are the electric current intensity, resistance and the conductance before and after gas exposure, respectively. If we assume that the mobility of electron, its relaxation time, and samples size (L and A) to be gas independent, then the sensitivity may be written as:

$$S = \frac{|\sigma_g - \sigma_a|}{\sigma_a} \times 100\% = \frac{|n_g - n_a|}{n_a} \times 100\% \qquad \text{(A-7)}$$

where n_g and n_a are the respective densities of electrons in presence and absence of gas. These densities should concern the electrons most responsible for conduction. As shown in Equation (A-3), and neglecting the variation of Fermi energy before and after the landing of a gas molecule on the sample, the sensitivity can be written as:

$$S = \frac{\left|N_F^{(g)} - N_F^{(a)}\right|}{N_F^{(a)}} \times 100\% \qquad \text{(A-8)}$$

where $N_F^{(g)}$ and $N_F^{(a)}$ are the density of states (DOS) at Fermi level with and without gas molecule, respectively. Furthermore, total DOS of either pristine graphene or CNT should be normalized (such as 8 electrons per hexagon) in order to keep a reference in dealing with ratio in Equation (A-8).

References

[1] Z. Liu, et al., Nature 524 (2015) 335.
[2] A.B. Rao, A.R. Rubin, Environ. Sci. Technol. 36 (2002) 4467.
[3] G.F. Fine, L.M. Cavanagh, A. Afonja, R. Binions, Sensors 10 (2010) 5469.
[4] P. Nugent, Y. Belmabkhout, S.D. Burd, A.J. Cairns, R. Luebke, Nature 495 (2013) 80.
[5] O. Shekhah, Y. Belmabkhout, Z. Chen, V. Guillerm, A. Cairns, K. Adil, M. Eddaoudi, Nat. Commun. 5 (2014) 4228.
[6] M.S. Shafeeyan, W.M.A. Wan Daud, A. Houshmand, A. Shamiri, J. Anal. Appl. Pyrolysis 89 (2010) 143.
[7] N. Zouadi, S. Messaci, S. Sam, D. Bradai, N. Gabouze, Mat. Sci. Semicond. Process. 29 (2015) 367.
[8] A.K. Mishra, S. Ramaprabhu, Energy Environ. Sci. 4 (2011) 889.
[9] H.J. Yoon, D.H. Jun, J.H. Yang, Z. Zhou, S.S. Yang, M.M. Cheng, Sens. Actuators B 157 (2011) 310.
[10] K.K. Paulla, A.A. Farajian, J. Phys. Chem. C 117 (2013) 12815.
[11] K. Sumida, et al., Chem. Rev. 112 (2012) 724.
[12] L.I. Bendavid, E.A. Carter, J. Phys. Chem. C 117 (2013) 26048.
[13] T. Zhu, E. Ertekin, Phys. Rev. B 91 (2015) 205429.
[14] T. Zhu, E. Ertekin, Phys. Rev. B 93 (2016) 155414.
[15] M. Rahimi, J.K. Singh, F. Muller-Plathe, J. Phys. Chem. C 119 (2015) 15232.
[16] S. Iihima, Nature 354 (1991) 56.
[17] M.S. Dresselhaus, G. Dresselhaus, P.C. Eklund, Science of Fullerenes and Carbon Nanotubes: Their Properties and Applications, Academic Press, New York,

NY, USA, 1996.

[18] C. Dekker, S. Trans, J. Sander, A. Verschueren, Nature 393 (1998) 49.
[19] R. Martel, T. Schmidt, H.R. Shea, T. Hertel, Ph Avouris, Appl. Phys. Lett. 73 (1998) 2447.
[20] H. Choi, H. Kim, S. Hwang, W. Choi, M. Jeon, Sol. Energy Mater. Sol. Cells 95 (2011) 323.
[21] P. Avouris, Z. Chen, V. Perebeinos, Nat. Nanotech. 2 (2007) 605.
[22] X. Li, X. Liu, J. Huang, Y. Fan, F. Cui, Surf. Coat. Technol. 206 (2011) 759.
[23] J.S. Jeong, H.W. Kee, Phys. Rev. B 80 (2009) 075409.
[24] T. Zhang, S. Mubeen, N.V. Myung, M.A. Deshusses, Nanotechnology 19 (2008) 332001.
[25] R.K. Roy, M.P. Chowdhury, A.K. Pal, Vacuum 77 (2005) 223.
[26] C. Lu, H. Bai, B. Wu, F. Su, F. Hwang, Energy Fuels 22 (2008) 3050.
[27] F. Su, C. Lu, W. Cnen, H. Bai, J.F. Hwang, Sci. Total Environ. 407 (2009) 3017.
[28] Y. Jin, S.C. Hawkins, C.P. Huynh, S. Su, Energy Environ. Sci. 6 (2013) 2591.
[29] M. Rahimi, D.J. Babu, J.K. Singh, Y.B. Yang, J.J. Schneider, F. Muller-Plathe, J. Chem. Phys. 143 (2015) 124701.
[30] S.S. Varghese, S. Lonkar, K.K. Singh, S. Swaminathan, A. Abdala, Sens. Actuators B 218 (2015) 160.
[31] G. Neri, Chemosensors 3 (2015) 1.
[32] A.K. Mishra, S. Ramaprabhu, J. Mater. Chem. 4 (2011) 889.
[33] Y. H. Zhang, J.L. Chen, Y. Zhou, F. Li, H. L. Zhang, (2016) Unpublished; H.-P. Zhang, X.-G Luo, H.-T. Song, X.-Y Lin, X. Lu and Y. Tang, Appl. Surf. Sci. 317, 2014, 511.
[34] T. Frauenheim, et al., J. Phys. Condens. Matter 14 (2002) 3015. www.dftb.org.
[35] P. Koskinen, V. Mäkinen, Comput. Mater. Sci. 47 (2009) 237.
[36] H.J. Monkhorst, J.D. Pack, Phys. Rev. B 13 (1976) 5188.
[37] J.C. Slater, G.F. Koster, Phys. Rev. 94 (1954) 1498.
[38] M. Elstner, D. Porezag, G. Jungnickel, J. Elsner, M. Haugk, Th Frauenheim, Phys. Rev. B 58 (1998) 7260.
[39] T.A. Niehaus, M. Elstner, Th Frauenheim, S. Suhai, J. Mol. Struct. Theochem. 541 (2001) 185.
[40] G. Zheng, H.A. Witek, P. Bobadova-Parvanova, S. Irle, D.G. Musaev, R. Prabhakar, K. Morokuma, M. Lundberg, M. Elstner, C. Kohler, T.J. Frauenheim, Theor. Comput. 3 (2007) 1349.
[41] C.M. Goringe, D.R. Bowler, E. Hernandez, Rep. Prog. Phys. 60 (1997) 1447.
[42] M. Elstner, Theor. Chem. Acc. 116 (2006) 316.
[43] P. Giannozzi, S. Baroni, et al., J. Phys. Condens. Matter 21 (2009) 395502.
[44] D. Vanderbilt, Phys. Rev. B 41 (1990) 7892–7895.
[45] J.P. Perdew, K. Burke, M. Ernzerhof, Phys. Rev. Lett. 77 (1996) 3865–3868.
[46] S. Grimme, J. Comput. Chem. 27 (2006) 1787–1799.
[47] V.I. Hegde, S.N. Shirodkar, N. Tit, U.V. Waghmare, Z.H. Yamani, Surf. Sci. 621 (2014) 168.
[48] S. Kouser, U.V. Waghmare, N. Tit, Phys. Chem. Chem. Phys. 16 (2014) 10719.
[49] N.W. Ashcroft, N.W. Mermin, in: D.G. Crane (Ed.), Solid State Physics, Harcourt College Publishers, New York, 1976, p. 29 (Chapter 2).
[50] J.M. Ziman, Principles of the Theory of Solids, second ed., Cambridge University Press, 1979, p. 211 (Chapter 7).
[51] A.I. Ayesh, J. Alloys Compd. 689 (2016) 1–5.
[52] A.I. Ayesh, A.F.S. Abu-Hani, S.T. Mahmoud, Y. Haik, Sens. Actuators B 231 (2016) 593.
[53] M. Abu-Haija, A.I. Ayesh, S. Ahmed, M.S. Katsiotis, Appl. Surf. Sci. 369 (2016) 443.